MITSUBISHI HEAVY INDUSTRIES, LTD.
16-5, KONAN 2-CHOME, MINATO-KU
TOKYO, JAPAN

September 8, 2011

Document Control Desk
U.S. Nuclear Regulatory Commission
Washington, DC 20555-0001

Attention: Mr. Jeffery A. Ciocco

Docket No. 52-021
MHI Ref: UAP-HF-11303

Subject: Equation for Ultimate Shear Strength of Reinforced Concrete Structures, as Referenced in the SMiRT Paper "1/10th Scale Model Test of Inner Concrete Structure Composed of Concrete Filled Steel Bearing Wall"

References: 1) NRC Request for 1/10th Scale Model Equation Reference

Reference 1 notes the U.S. Nuclear Regulatory Commission ("NRC") staff request to MHI, requesting the reference which supports the equation for ultimate shear strength of reinforced concrete (RC) structures used in document entitled "References for 1/10th Scale Model Test of Inner Concrete Structure Composed of Concrete Filled Steel Bearing Wall". The NRC has stated that this request supports their review of MUAP-11013 and MUAP-11018.

With this letter, Mitsubishi Heavy Industries, Ltd. ("MHI") transmits to the NRC the reference for the ultimate shear strength equation as used in document entitled "References for 1/10th Scale Model Test of Inner Concrete Structure Composed of Concrete Filled Steel Bearing Wall". The document is included in the Transactions for the 10th International Conference on Structural Mechanics in Reactor Technology (SMiRT).

The enclosed reference is based on the Abstracts of the Annual Congress of the AIJ, and contains the following Parts 1 through 6:

- Evaluation Method for Restoring Force Characteristics of R/C Shear Walls of Reactor Buildings: (Part 1) Evaluation Method for Restoring Force Characteristics
- Evaluation Method for Restoring Force Characteristics of R/C Shear Walls of Reactor Buildings: (Part 2) Referred Test Data
- Evaluation Method for Restoring Force Characteristics of R/C Shear Walls of Reactor Buildings: (Part 3) Shear Stress – Shear Strain Skeleton Curve
- Evaluation Method for Restoring Force Characteristics of R/C Shear Walls of Reactor Buildings: (Part 4) Moment-Curvature Skeleton Curve
- Evaluation Method for Restoring Force Characteristics of R/C Shear Walls of Reactor Buildings: (Part 5) Fitness Evaluation of the Computed Skeleton Curves with Experimental Data
- Evaluation Method for Restoring Force Characteristics of R/C Shear Walls of Reactor Buildings: (Part 6) Hysteresis

D081
NRO

Please contact Dr. C. Keith Paulson, Senior Technical Manager, Mitsubishi Nuclear Energy Systems, Inc. if the NRC has questions concerning any aspect of this letter. His contact information is provided below.

Sincerely,

Y. Ogata

Yoshiki Ogata,
General Manager- APWR Promoting Department
Mitsubishi Heavy Industries, LTD.

Enclosure:

1. Evaluation Method for Restoring Force Characteristics of R/C Shear Walls of Reactor Buildings: (Parts 1-6)

CC:J. A. Ciocco
C. K. Paulson

Contact Information
C. Keith Paulson, Senior Technical Manager
Mitsubishi Nuclear Energy Systems, Inc.
300 Oxford Drive, Suite 301
Monroeville, PA 15146
E-mail: ck_paulson@mnes-us.com
Telephone: (412) 373-6466

Docket No. 52-021
MHI Ref: UAP-HF-11303

Enclosure 1

UAP-HF-11303
Docket No. 52-021

Evaluation Method for Restoring Force Characteristics of R/C Shear Walls of Reactor Buildings: (Parts 1-6)

September, 2011

2145

Evaluation Method for Restoring Force Characteristics of R/C Shear Walls of Reactor Buildings

(Part 1) Evaluation Method for Restoring Force Characteristics

Shigeru Furukawa[*1] (member), Hiroshi Tanaka[*1] (member)
Katsuyoshi Imoto[*2] (member), Seiji Yoshizaki[*3] (member)

1. Introduction

In the aseismic design of reactor buildings, elastic-plastic seismic response analysis is performed to investigate the safety of the building and evaluate the seismic input to equipment and piping systems. It is therefore preferable that the restoring force characteristics used for response analysis are easy to handle computationally while at the same time representing the ultimate behavior of the buildings as faithfully as possible.

Previous methods for the evaluation of restoring force characteristics have largely relied on computation formulas based on experimental data for ordinary buildings. However, in recent years a large number of model tests have been performed on shear walls of nuclear reactor buildings, resulting in the accumulation of substantial experimental data and many new findings relating to restoring force characteristics.

In this report, we review the previous experimental data available in Japan based on these findings, and we set up a standard method for the evaluation of restoring force characteristics used in the elastic-plastic seismic response analysis of reinforced concrete (R/C) buildings.

2. Method for the Evaluation of Restoring Force Characteristics

Seismic response analysis of reactor buildings is usually performed using a lumped mass model. With the model, it is possible to separately evaluate the restoring force characteristics of shear walls by dividing them into a shear stress vs. shear strain

relationship (hereinafter referred to as a τ - γ relationship) and a bending moment vs. bend curvature relationship (hereinafter referred to as a M-ϕ relationship). The corresponding skeleton curves and hysteresis characteristics are determined in the following way.

1) The skeleton curves are displayed as line graphs for both the τ - γ and M-ϕ relationships, with each turning point and ultimate point calculated according to the following formula.

(a) τ - γ relationship (see Fig. 1)

(b) M- ϕ relationship (see Fig. 2)

2) The hysteresis characteristics are set by applying the following rules to the τ - γ and M-ϕ relationships:

(a) τ - γ relationship (see Fig. 3)

1. For maximum-point-oriented hysteresis, if the recovery after the peak value has passed the first turning point does not exceed the first turning point on the opposite side, then the system moves along a straight line connecting the peak value with the first turning point on the opposite side.
2. The stable loop has no area.

(b) M-ϕ relationship (see Fig. 4)

1. Assumed to be maximum-point-oriented.
2. In the second rigid zone, the stable loop has no area.
3. In the third rigid zone, the stable loop is a degrading trilinear type with a parallelogram that provides equivalent viscous damping corresponding to the maximum curvature. The vertices of the parallelogram are the points obtained by subtracting $2M_1$ from the peak value.
4. The recovery after the peak value has exceeded the second turning point forms a stable loop with its minimum value at the second turning point on the opposite side if the displacement of the opposite side has not exceeded the second turning point.

5. The stiffness used for repetition inside the stable loop is assumed to be equal to the recovery stiffness of the stable loop.

3. Considerations for Practical Application

1) The evaluation formula is set based on model tests of reactor buildings. When applying this formula, it is crucial to ensure that the range and composition of these structural factors do not depart from those of the model.

2) When considering the effects of an opening, rules such as those given in Section 4, Article 18 of the Architectural Institute of Japan document "Annotated R/C Structural Design Standards," can be applied with modifications.

3) When applying this evaluation method to prestressed concrete shear walls that use unbonded tendons, the prestress is handled as an axial compression, and the PC steel members can be ignored.

4) The stiffness of cylindrical shear walls subject to internal pressure tends to be lower from the early stages compared with this evaluation method. In setting the restoring force characteristics of this sort of shear wall, the characteristics must be examined with reference to experimental data. In a prestressed concrete containment vessel, the effect from internal pressure may be disregarded because the prestress is introduced to cancel out the internal pressure.

5) The physical properties of concrete may change when exposed to particularly high temperatures, possibly affecting the restoring force characteristics, thus it is crucial to consider the implications of this effect.

4. Summary

This evaluation method is simple to use in seismic response analysis and is compatible with the results from the reactor building shear wall model tests as shown in the investigation results of (Part 2) through (Part 6),

This report was produced as part of the research into evaluation methods for seismic margins in reactor buildings conducted by 10 power generating businesses comprising the Joint Power Generating Research Initiative.

[Acknowledgements] This study was greatly assisted by Chairman Tsuneo Okada and the members of the research committee for evaluation methods for earthquake resistance margins in reactor buildings. Thank you all very much for your help.

*1: The Tokyo Electric Power Company
*2: Obayashi Corporation
*3: Taisei Corporation

(a) τ - γ relationship

First turning point

$$\tau_1 = \sqrt{\sqrt{Fc}\ (\sqrt{Fc} + \sigma_v)} \quad (1)$$

$$\gamma_1 = \tau_1 / G \quad (2)$$

Second turning point

$$\tau_2 = 1.35\ \tau_1 \quad (3)$$

$$\gamma_2 = 3\gamma_1 \quad (4)$$

Ultimate point

$$\tau_3 = \{1 - \tau_s / (4.5\sqrt{Fc})\}\ \tau_0 + \tau_s \quad (\tau_s \leqq 4.5\sqrt{Fc}) \quad (5\text{-}1)$$

$$= 4.5\sqrt{Fc} \quad (\tau_s > 4.5\sqrt{Fc}) \quad (5\text{-}2)$$

$$\gamma_3 = 4.0 \times 10^{-3} \quad (6)$$

$$\tau_0 = (3 - 1.8\ M/QD)\sqrt{Fc}$$

except if M/QD>1 then M/QD=1

$$\tau_s = (p_v + p_H)_s \sigma_y / 2 + (\sigma_v + \sigma_H) / 2$$

(b) M-ϕ relationship

First turning point

$$M_1 = Ze(f_t + \sigma_v) \quad (7)$$

$$\phi_1 = M_1 / (cE \cdot Ie) \quad (8)$$

Second turning point

$$M_2 = My \quad (9)$$

$$\phi_2 = \phi_y \quad (10)$$

Ultimate point

$$M_3 = Mu \quad (11)$$

$$\phi_3 = 0.004 / Xnu \quad (12)$$

except if $\phi_3 > 20\phi_2$ then $\phi_3 = 20\phi_2$

F_c : Compressive strength of concrete (kg/cm^2)

G : Shear modulus of concrete (kg/cm^2)

$_cE$: Young's modulus of concrete (kg/cm^2)

P_v, P_H : Vertical and horizontal reinforcement ratio (real number)

σ_v, σ_H : Vertical and horizontal axial stress (kg/cm^2) (compression is positive)

$_s\sigma_y$: Reinforcement yield stress (kg/cm^2)

M/QD : Shear span ratio(-)

I_c : Geometrical moment of inertia, taking reinforcement into consideration (cm^4)

Z_c : Section modulus, taking reinforcement into consideration (cm^3)

$f_t = 1.2\sqrt{F_c}$: Bending tensile strength of concrete (kg/cm^2)

M_y : Moment at tensile yield of reinforcement (kg·cm)

ϕ_y : Curvature at tensile yield of reinforcement (1/cm)

D : Center-to-center distance of tension and compression flanges (cm)

M_u : Fully plastic moment (kg·cm)

X_{nu} : Distance from extreme compression fiber to central axis at fully plastic moment (cm)

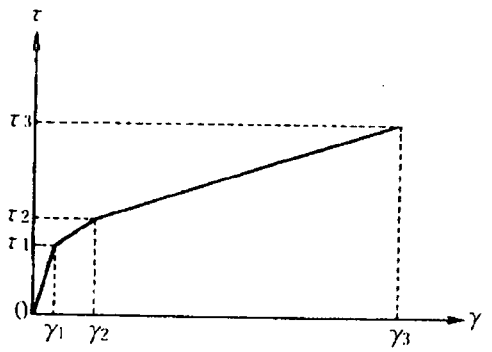

Fig.1 Skeleton curve of τ - γ relationship

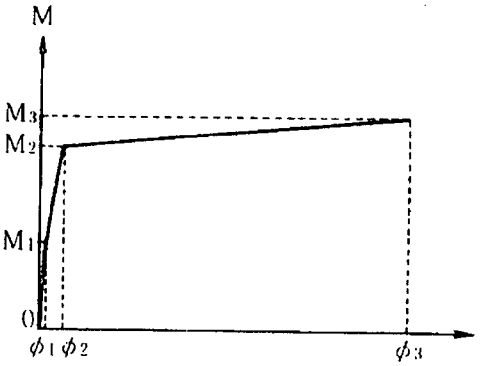

Fig. 2 Skeleton curve of M-ϕ relationship

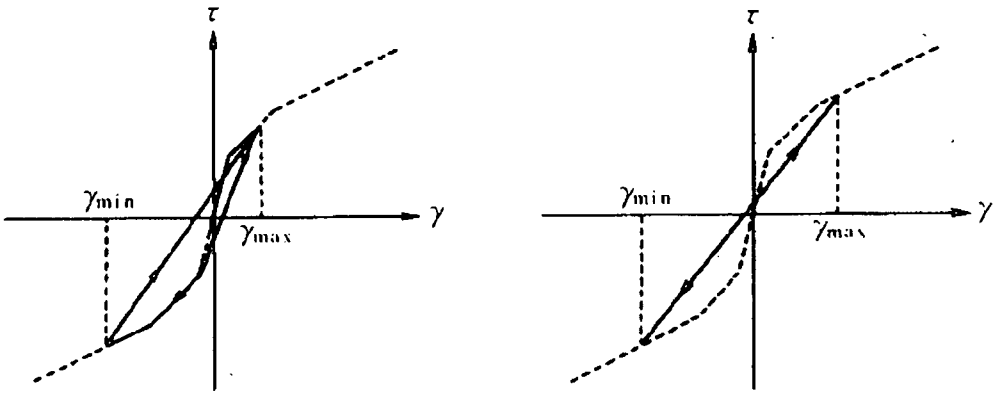

(i) Transient state (in 2nd and 3rd rigid zones)

(ii) Steady state (in 2nd and 3rd rigid zones)

Fig. 3 Schematic diagram of hysteresis characteristics of τ - γ relationship

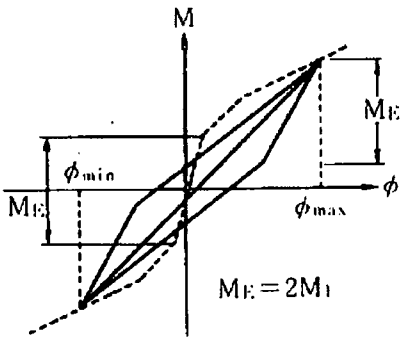

(a) Stable loop (in third rigid zone)

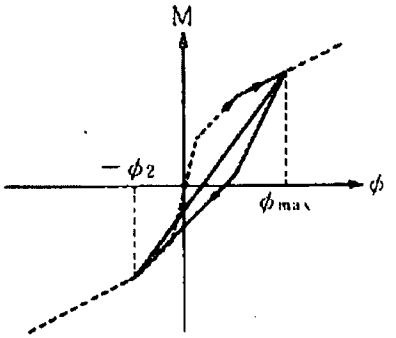

(b) Transient loop (when $\phi_{max} > \phi_2$ for the first time)

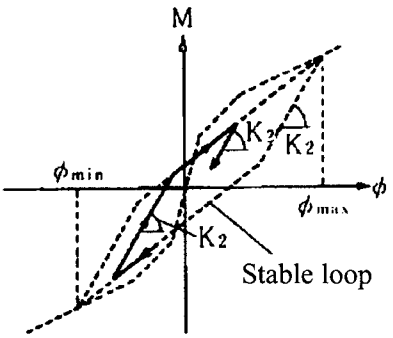

(c) Rule inside stable loop ($\phi_{min} > \phi > \phi_{max}$)

Fig. 4: Schematic diagram of hysteresis characteristics of M- ϕ relationship

2146

Evaluation Method for Restoring Force Characteristics of R/C Shear Walls of Reactor Buildings

(Part 2) Referred Test Data

Seiji Yoshizaki[*1] (member), Hiroshi Tanaka[*2] (member)

1. Introduction

Data from previous experiments were investigated to cross-examine the suitability of the restoring force characteristics and experimental data set in (Part 1). This report discusses the scope of the data collected.

2. Previous experiments

Experimental studies of horizontal loading applied to shear walls of reactor buildings are listed in the <References> section. Such experiments were mainly performed by extracting the primary aseismic elements of buildings. For BWR-type buildings, experiments are performed on cylindrical or truncated conical shield walls, or box walls. For PWR-type buildings, experiments were performed on cylindrical walls used as external shielding walls, cylindrical walls subjected to prestressing forces and internal pressure to simulate a PCCV, and octagonal walls without considering the four-loop secondary shielding wall.

There have also been many tests performed on I-section walls which are common to both types of building.

3. Scope of data collected

103 total test structures were examined, comprised of 22 box walls, 26 RC cylindrical walls, 19 cylindrical walls subjected to prestressing or internal pressurization, 3 truncated conical walls, 9 octagonal walls, and 24 I-section walls.

The majority of the test structures were sized from 1/10 to 1/30 scale of the actual structures, at flange center-to-center distance (D) of 100–200 cm and the wall thickness

(t) of 5–10 cm, as shown in Figs. 1 and 2. As shown in Fig. 3, the shear span ratios (M/QD) were split equally between the ranges of 0.5–1.0 and 1.0–1.5.

The compressive strength of concrete (Fc) and the yield strength of reinforcing bars are shown in Figs. 4 and 5, with the common compressive strength of concrete in the range of 240–260 kg/ cm^2. Although many test cases had values in excess of 400 kg/cm^2, they were test structures for PCCV. Reinforcing bars are commonly made from SD35, but there were also many experiments where SD40 was used. The strengths of these materials correspond to those of the actual structures.

The reinforcement ratios are shown in Fig. 6. Since the test structures had different vertical and horizontal reinforcement ratios, these ratios are shown separately. From these figures, the peak reinforcement ratios were confirmed at 1.2% or less, which is consistent with the reinforcement ratio of actual structures, though there are also many test structures with higher reinforcement ratios.

4. Separation of Deformation Components

Restoring force characteristics are evaluated by the shear stress vs. strain relationship and the bending moment vs. curvature relationship. To apply the test data to this evaluation, the separation of the deformation components from the test data into shear deformation and bending deformation components were required.

In test structures where measurements were made of the curvature distribution in the height direction of the wall, it is possible to calculate the bending deformation from the bending distribution according to Fig. 8, and the shear deformation can be obtained by subtracting the bending deformation from the overall deformation.

$$\delta_B = \sum_{i=1}^{n} \{(\Delta\delta_{Li} - \Delta\delta_{Ri}) \times dHI/L\}$$

Figure 7 shows the extent of data from this viewpoint for each planar shape. Of the 103 test structures, there were 48 for which it was possible to obtain information down to the loop for each type of deformation, and 67 for which it was possible to investigate the skeleton for each deformation component. The remaining 23 structures were only used for an investigation of the maximum loads.

5. Summary

By analyzing past experimental data, it was proven that the structural elements of actual reactor buildings are adequately covered with regard to factors such as the shear span ratio, concrete compressive strength, reinforcement yield point, reinforcement ratio and test structure shape.

<References>

1. Akino et al.: "Tests of restoring force characteristics in reactor buildings (Parts 1–7)," 1982 AIJ Annual Meeting
2. Kogaki: "A study of shear strength in prestressed concrete cylindrical walls, Parts 1-5," 1979 AIJ Annual Meeting
3. Umemura et al.: "An experimental study of strength and restoring force characteristics of reinforced concrete earthquake-resisting walls (Parts 1–3)," AIJ Kanto Regional Group, 1976
4. Nagashima et al.: "A study of cylindrical RC earthquake-resistant walls," AIJ Kinki Regional Group, 1979
5. Ohagi et al.: "A study of restoring force characteristics of reinforced concrete earthquake-resisting walls," Kansai Electric Power Research Institute, 1982
6. Kogaki et al.: "Structural strength tests of a prestressed concrete containment vessel based on 1/8 and 1/30 scale models," Prestressed Concrete, 1981
7. Uchida et al: "Scale model tests of internal pressure and simultaneous horizontal loading in reinforced concrete containment vessels for nuclear power stations, Parts 1–6," 1978–1980 AIJ Annual Meetings

8. Suzuki et al.: "Horizontal loading tests on reactor buildings, Parts 1 & 2,", 1980 AIJ Annual Meeting
9. Yano et al.: "An experimental study of the structural characteristics of large-diameter reinforcement joints," 1985 AIJ Annual Meeting
10. Endo et al.: "An experimental study of the mechanical properties of box walls with forces applied in two directions," 1985 AIJ Annual Meeting
11. Sakamoto et al.: "A study of the restoring force characteristics of buildings, Parts 2–5," 1983 AIJ Annual Meeting
12. Kasega et al.: "A study of the restoring force characteristics of buildings, Parts 6 & 7," 1983 AIJ Annual Meeting
13. Machida et al.: "Horizontal loading tests of cylindrical prestressed concrete walls, Parts 1–3," 1983 AIJ Annual Meeting
14. Okamura et al.: "Horizontal loading tests of concrete reactor containment vessel models, Parts 1–4," 1979 and 1980 AIJ Annual Meetings
15. Okada et al.: "Tests of restoring force characteristics in reactor buildings (Parts 1–6)," 1986 AIJ Annual Meeting
16. Yajima et al.: "An experimental study of earthquake-resisting walls using high strength concrete (Parts 3 & 4)," 1986 AIJ Annual Meeting

*1: Taisei Corporation
*2: The Tokyo Electric Power Company

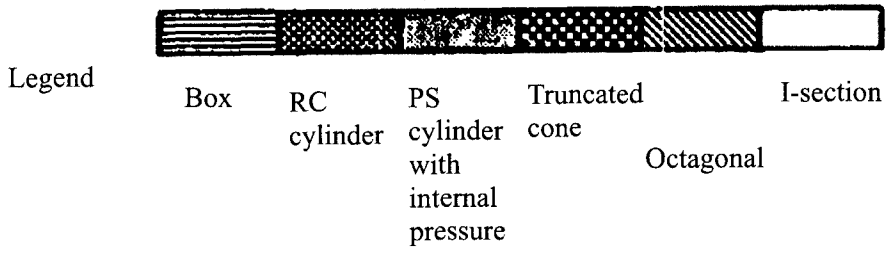

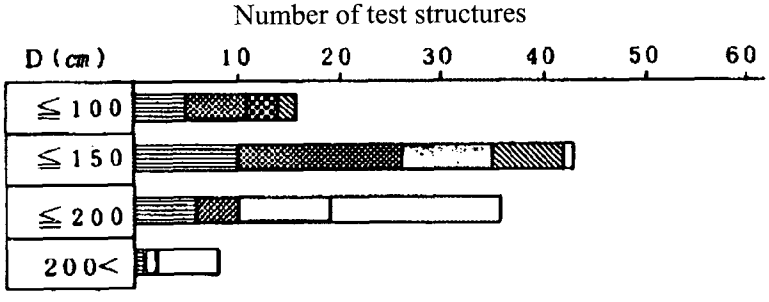

Fig. 1: Distribution of wall lengths

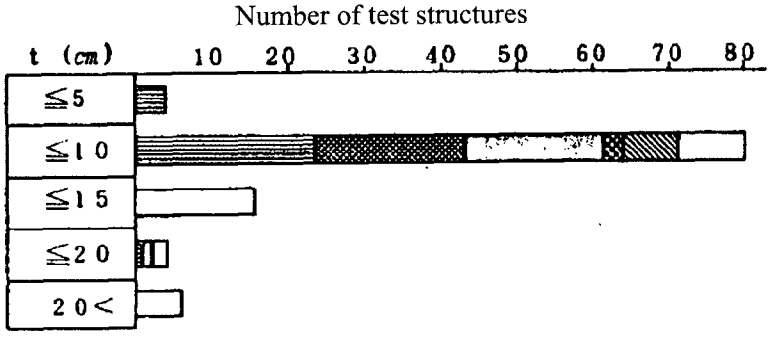

Fig. 2: Distribution of wall thicknesses

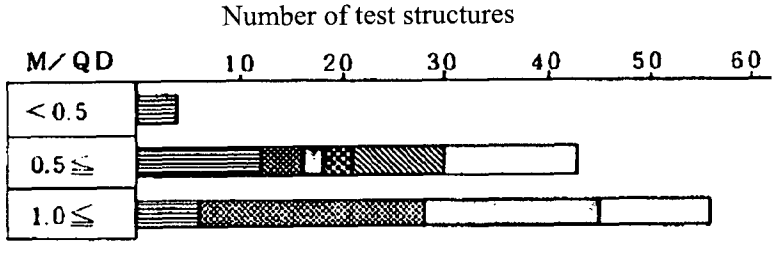

Fig. 3: Distribution of shear span ratios

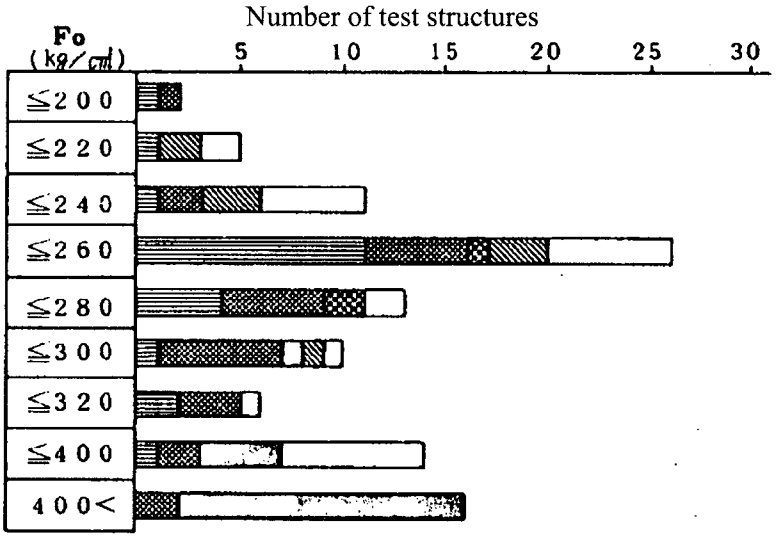

Fig. 4: Distribution of concrete compressive strengths

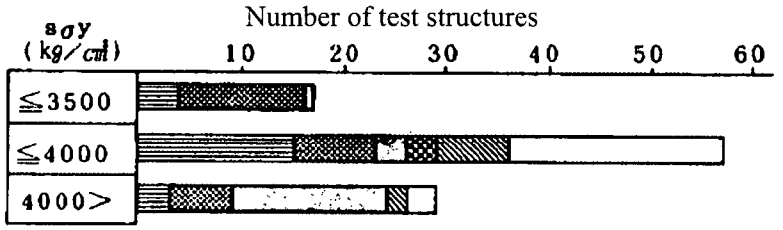

Fig. 5: Distribution of reinforcing bar yield strength

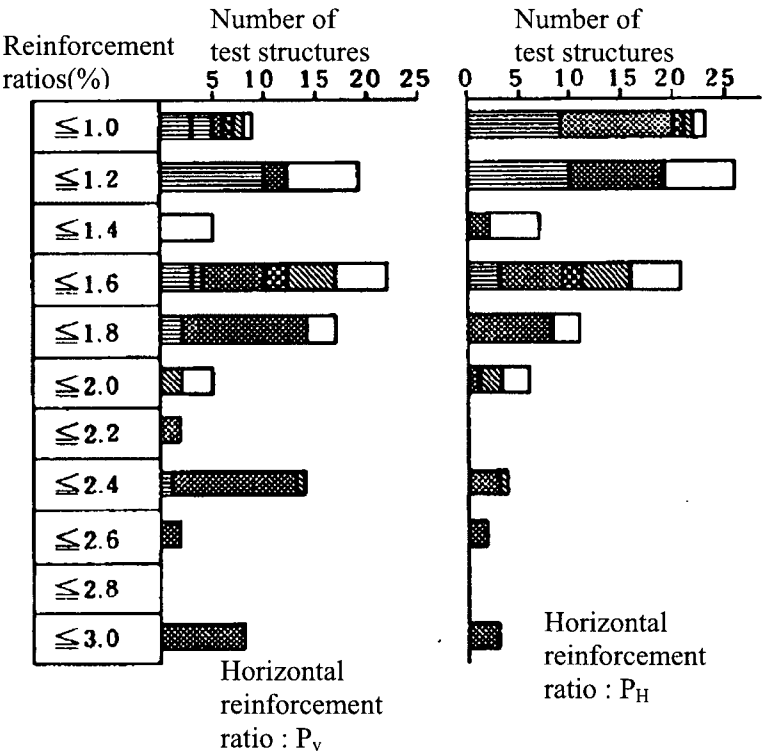

Fig.6 Distribution of reinforcement ratios

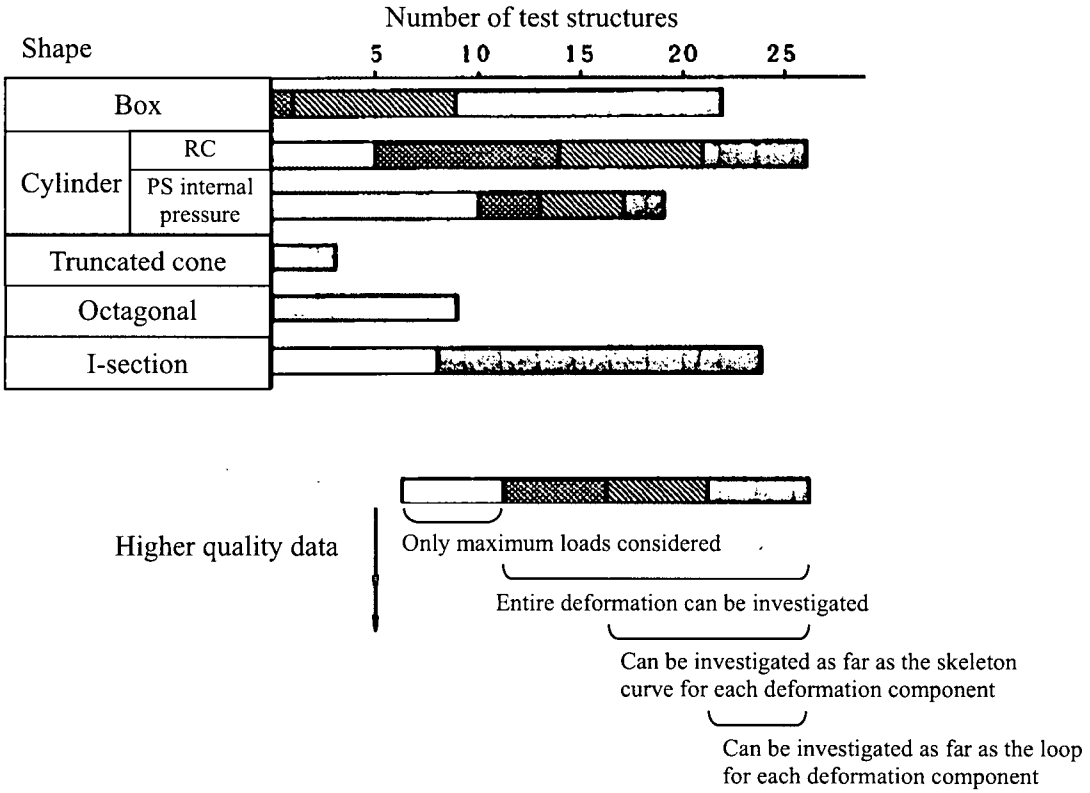

Fig. 7 Data quality

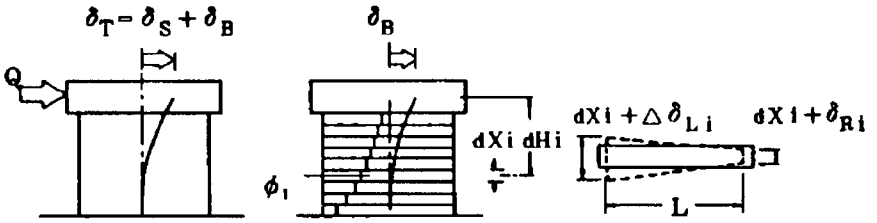

Fig.8 Determination of bending deformation

2147

Evaluation Method for Restoring Force Characteristics of R/C Shear Walls of Reactor Buildings

Part 3: Shear Stress – Shear Strain Skeleton Curve

Yasuo Inada[*1] (member), Hiroshi Tanaka[*2] (member)

1. Introduction

This report discusses the rationale for the setting of formulae for calculating the τ - γ relationship from among the restoring force skeleton curve evaluation methods proposed in (Part 1), and discusses the results of comparing them with the experimental data shown in (Part 2).

2. Rationale for Setting Formula and Comparison with Experimental Data

The calculated values of the τ - γ skeleton curves are obtained from Equations (1) through (6) presented in (Part 1). The effective cross-sectional area used for shear stress calculations is taken as the cross-sectional area of the web for box walls and I-section walls, and half the overall cross-sectional area for other types.

The experimental and calculated values are compared in Table 1.

Table 1: Ratio of experimental to calculated values for turning points of the τ - γ relationship and initial stiffness

		Number of data	Mean	Std. deviation
Shear stress at first turning point	All data	57	0.98	0.21
	Except (i), (ii) and (iii)	51	0.98	0.18
Initial stiffness	All data	49	0.93	0.16
	Except (i), (ii) and (iii)	42	0.94	0.16
Shear stress at second turning point	All data	58	0.99	0.17
	Except (iv)	51	1.00	0.17
Shear stress at ultimate point	All data	86	1.04	0.19
	Except (iv)	75	1.01	0.15
Shear strain at ultimate point	All data	48	1.74	0.76
	Except (iv)	37	1.08	0.82

N.B.: Special Conditions

(i) Box wall test structure with diagonally applied force

(ii) Test structure using mortar

(iii) PCCV test structure

(iv) Test structure including bend reinforcing bars in the flange

As the computation formula for the first turning point, Equation (1)[ref1] was used to evaluate the average shear stresses during the occurrence of oblique center cracks in shear tests of the of the inner surface of wall plates. As shown in Table 1 and Fig. 1, the average ratio of the experimental and calculated values is 0.98, indicating a close agreement. The variation is small except under special conditions. The turning point 1 shear strain calculation formula (2) determines the initial stiffness of the τ - γ relationship as the shear modulus G of concrete. In the comparison of initial stiffness between Table 1 and Fig. 2, the experimental values were found to be slightly lower.

Looking at the actual τ - γ relationship, the stiffness gradually decreases after the vicinity of where the cracking occurs, resulting in a convex curvature. To simulate this behavior, we set γ_2 at three times the position of γ_1, and we read the value of τ at this time from the experimental curve to obtain the ratio β of this value to τ_1. The

results are shown in Fig. 3 and Table 2. The value of β is 1.35 except under special conditions, and Equation (3) is determined from this value.

As the formula for calculating the shear stress at the ultimate point, we used the proposed Equation (5)[ref.2] where the load carried by the reinforcing bars is expressed by a full reinforcement formula, and the load carried by the concrete is also taken into consideration. As shown in Table 1 and Fig. 4, the average ratio of the experimental and calculated values is 1.04, and the variation is also small. Furthermore, the test structures in which large numbers of vertical reinforcements were arranged in the flange wall of an I-section wall showed consistency with both the mean and standard deviation values, except for the excluded conditions which are not normally seen in real equipment.

The ultimate shear strain is determined by Equation (6) [ref.3] by considering data for ordinary shear walls. Table 3 shows the ultimate shear strain determined experimentally for each test structure shape. Figure 5 shows an example of the actual values for the skeleton curve of the τ - γ relationship. The curve consists of an initial linear section, followed by a convex curved section and then a more or less flat section after the maximum strength has been reached. This flat section is relatively short for box walls and I-section walls, and long for other shapes. However, considering the large variation in experimentally measured values of ultimate shear strain and the fact that the differences in the ultimate shear strain between wall shapes have not yet been fully clarified in theory, it was decided to model the parts before the flat section using a line graph with three turning points, and we used a uniform strain value of 4×10^{-3}. Figure 5 compares some examples of curves obtained from experimental and calculated values. For a box wall, the experimental and calculated values agree up to the maximum strength, and similarly for a cylindrical wall a close agreement is seen between the experimental and calculated values almost all the way up to the maximum strength. However, for cylindrical walls, the deformation continues after this point and thus the experimental values become very large relative to the values obtained by the proposed formula as shown in Fig. 6 and Table 3.

3. Summary

The rationale for the setting of the skeleton curve computation formula for the τ - γ relationship was demonstrated, and the comparison of this formula with experimental data was presented. The setting model is a line graph with three turning points, with the calculated values of τ and γ at the first turning point, second turning point and maximum point showing a close match with the average values of the experimental data. In the experimental skeleton curves for cylindrical walls, octagonal walls and the like, since there was an additional flat section after approaching maximum strength in the vicinity of the maximum strain set here, the experimental values of the ultimate shear strain are larger than the set values. This is an issue requiring further study.

<References>

1. Inada: "A Study of Restoring Force Characteristics of Earthquake-Resisting Walls for Reactor Buildings," AIJ Society Report, January 1987 S62
2. Yoshizaki et al.: "Strength of Earthquake-Resisting Walls Having Large Numbers of Small Holes," Collected Papers of the 5th Concrete Research and Technology Conference, 1983
3. Tomii: "Materials on Ultimate Strength Design of Reinforced Concrete: 31," Journal of architecture and building science, July 1982

*1: Shimizu Corporation

*2: The Tokyo Electric Power Company

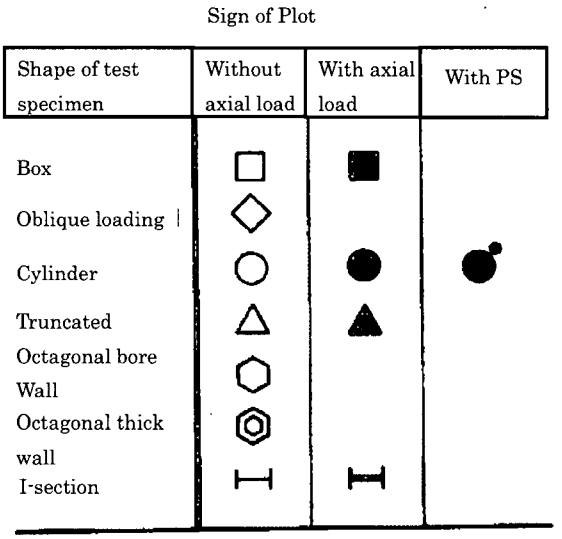

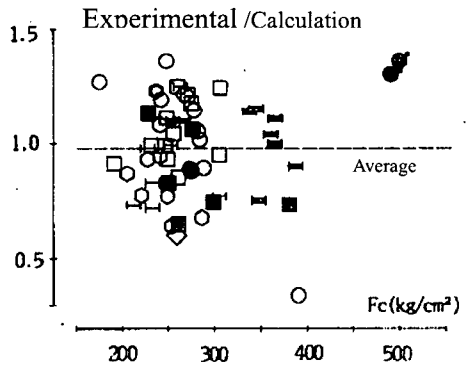

Fig. 1 Comparison of τ at first turning point

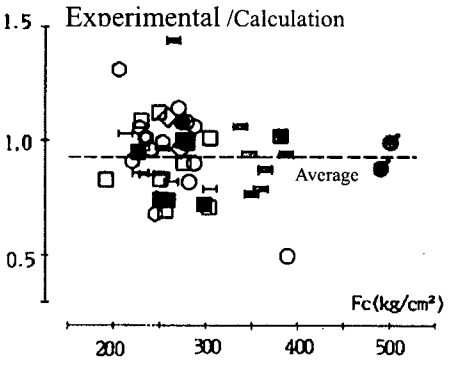

Fig. 2 Comparison of initial stiffness

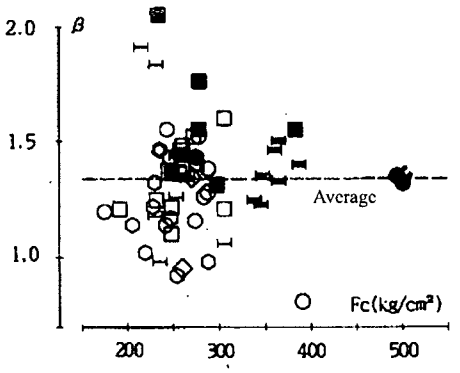

Fig. 3 Distribution of β values obtained from experimental data

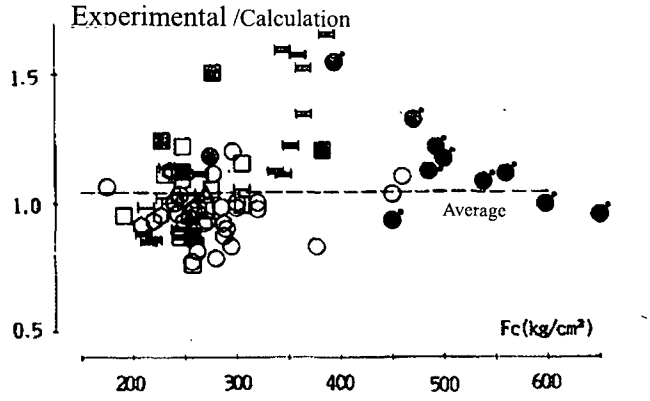

Fig. 4 Comparison of τ at ultimate points

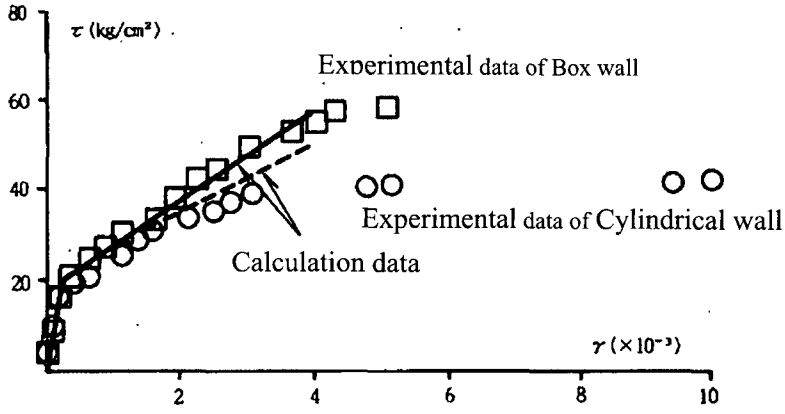

Fig. 5 Example of a skeleton curve for the τ - γ relationship

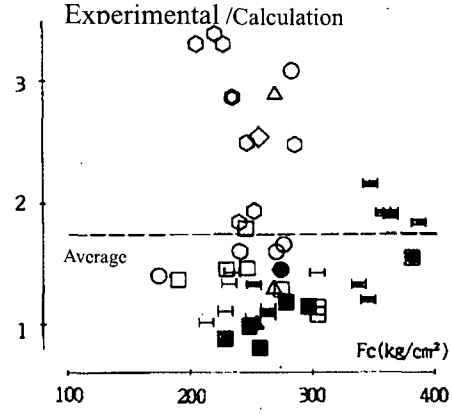

Fig. 6 Comparison of γ at ultimate points

Table 2 Average values of β obtained experimentally

	Number of data	Average
All data	58	1.34
Except data ①,②,③	51	1.35

Table 3 Shear strain at maximum strength for each test structure (units: $\times 10^{-3}$)

	Number of data	Average	Standard deviation	Coefficient of variation
Box Wall, I-section Wall	29	5.36	1.38	0.26
Cylindrical wall, Octagonal wall	15	9.77	3.17	0.32
Truncated conical wall, Oblique box wall	4	7.68	3.68	0.46
Total	15	9.77	3.02	0.44

2148

Evaluation Method for Restoring Force Characteristics of R/C Shear Walls of Reactor Buildings

Part 4 : Moment-Curvature Skeleton Curve

Hideo Nanba[*1] (member), Hiroshi Tanaka[*2] (member)

1. Introduction

This report will discuss the rationale of the standard Equations for calculating the M-ϕ relationship skeleton curve from among the evaluation methods for Restoring Force Characteristics proposed in (Part 1), and discus the results of comparing them with the experimental data shown in (Part 2).

2. Rationale for Setting Equations and Comparison with Experimental Data

The calculated values of the first turning point(M_1, ϕ_1), second turning point (M_2, ϕ_2) and Ultimate point (M_3, ϕ_3) into skeleton curves of the M-ϕ relationship are obtained from Equations (7) through (12) shown in (Part 1). The comparison of experimental values and calculated values used the experimentally determined bending moment of concrete footings and the angle of bending deformation (R_B). As shown in Fig. 1, the experimental values used here were the initial stiffness and the stiffness values at the each turning point and Ultimate points when approximating the skeleton curve of the M-R_B relationship by a polygonal line with three vertices. The comparison results are shown in Table 1. Since the experimental bending deformation values include additional deformation due to the extension of reinforcing bars from the substructure at the concrete footings, these were computationally evaluated as rotational deformations as proposed by Kotani (Ref. 1).

Table 1: Ratios of experimental to calculated values for vertices of the M-R_B relationship and initial stiffness

		Number of Specimens	Mean	Standard deviation
M_1	Load at first bending cracks	68	0.87	0.29
	Moment at first turning point of the three-turning point polygonal line approximation of experimental values	50	1.10	0.25
Initial stiffness		41	0.93	0.35
M_2	Moment at second turning point of the three-turning point polygonal line approximation of experimental values	36	1.07	0.17
R_{B2}	Angle of bending deformation at third turning point of the three-turning point polygonal line approximation of experimental values	36	1.44	0.54
M_3	Ultimate load	18	1.09	0.15

The bending moment at the first turning point (M_1) calculated using Equation (7) was determined according to the axial stress by taking the stress in edge of tension at the First bending cracks to be $1.2\sqrt{}Fc$ according to the description given in Article 8 of the AIJ Standard for Structural Calculation of Reinforced Concrete Structures. Figure 2 compares the calculated values with the experimental loads at first bending cracks. Also, Fig. 3 compares the experimental values of the M-R_B relationship with calculated values. The average values of the experimental and calculated values (abbreviated to (experimental)/(calculated) below) are 0.87 and 1.10 respectively as shown in Table 1. The calculated values were slightly larger than the experimental loads at first bending cracks, but the calculated values were lower than the bending moments at the first turning point of the M-R_B relationship.

In Equation (8) used for calculating the curvature at the first turning point (ϕ_1), the initial stiffness of the skeleton curve of the M- ϕ relationship is expressed in cE-Ie from the Young's modulus (cE) and the second moment of area (Ie). Ie is calculated in consideration of the effective width of flanges and reinforcing bars. The calculated value is compared with the gradient of the data prior to the first bending cracks as an experimental value of the initial stiffness. As shown in Fig. 4, the average

(experimental)/(calculated) ratio was 0.93, so the experimental values were slightly lower.

The Equation (9) for the bending moment at the second turning point (M_2) is obtained as the moment at yield of the reinforcing bars, and the calculated value is obtained by the following assumptions: ① the beam theory is applied, ② the σ -ε relationship of concrete is linear and the gradient equal to the Young's modulus, ③ the σ -ε relationship of reinforcing bars is linear to the yield point, and ④ the reinforcing bars are grouped in the middle of the wall. As shown in Fig. 5, the average (experimental)/(calculated) ratio is 1.07, which indicates a close representation.

The Equation (10) for the curvature (ϕ_2) at the second turning point is obtained as the bending curvature at the point of tensile yield of the reinforcing bars. As shown in Fig. 6, the average (experimental)/(calculated) ratio is 1.44, which shows that the experimental values tend to be larger.

The computation Equation (11) for the Ultimate point bending moment (M_3) is obtained as the moment of the concrete on the compression at the point of bending collapse. M_3 is calculated as the fully plastic moment by making the following assumptions: ① the stress in the concrete on the compressive side follows a rectangular distribution of 0.85Fc, ② the stress in the reinforcing bars is the yield stress ($s\sigma y$) on the tension side and $-s\sigma y$ on the compressive side, and ③ the reinforcing bars are grouped in the middle of the wall. Since there were few test structures that clearly reached the ultimate state of bending, the experimental values of test structures at the bending crash computationally are compared in Fig. 7. The average (experimental)/(calculated) ratio is 1.09, which s which indicates a close representation.

The Equation (12) for the bending curvature at the Ultimate point (ϕ_3) is determined by assuming that the strain in the concrete at the edge of compression is 0.004. If the axial force of the wall is small and the reinforcement ratio is relatively low, a neutral axis may exist inside the flange wall on the compressive side, resulting in an extremely large value. Since it is also possible to consider cases that the experiment cannot simulate properly, an upper limit of 20 ϕ_2 was applied.

3. Summary

The rationale for setting the Equations for calculating each turning point of the skeleton curve of the M- ϕ relationship was presented, and the results of comparing the calculated values with experimental data with regard to the relationship between bending moments and the angle of deformation members was demonstrated. The experimental values and calculated values match fairly well with regard to the initial stiffness and the moments at the first and second vertices and at the Ultimate point, but the experimentally measured deformation in the vicinity of the second turning point tended to be larger than the calculated value. Also, the ratio of the experimental and calculated values varies somewhat more than the τ - γ relationship. However, in the deformation of earthquake-resisting walls in reactor buildings during an earthquake, the proportion of bending deformation is generally small, and the proposed evaluation method shall be sufficient for practical applications.

<References>

1. Shunsuke Otani: "Inelastic Analysis of R/C Frame Structures," Journal of the Structural Division, July 1974, pp. 1433–1449, 2. ACI Committee 318: "Commentary on Building Code Requirements for Reinforced Concrete (ACI318-77)," American Concrete Institute pp. 39–43

*1: Takenaka Corporation

*2: The Tokyo Electric Power Company

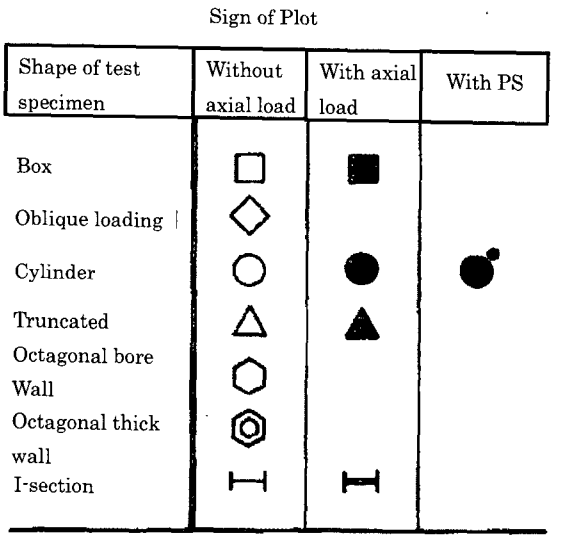

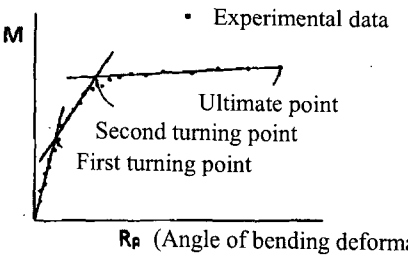

Fig.1 Approximating the experimental values with a three-turning point polygonal line

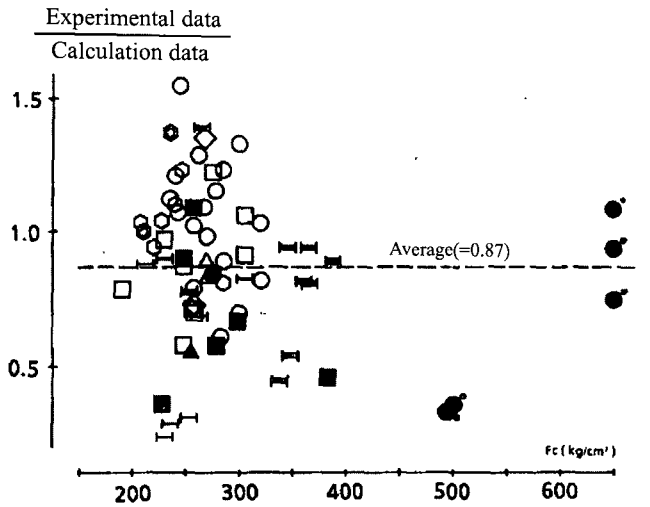

Fig.2 Comparison of first turning point M_1
(Load at which bending cracks are discovered)

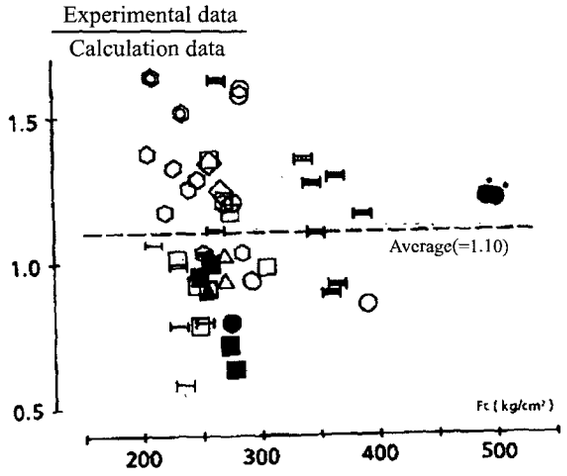

Fig.3 Comparison of first turning point M_1 (three-turning point polygonal line approximation of experimental values)

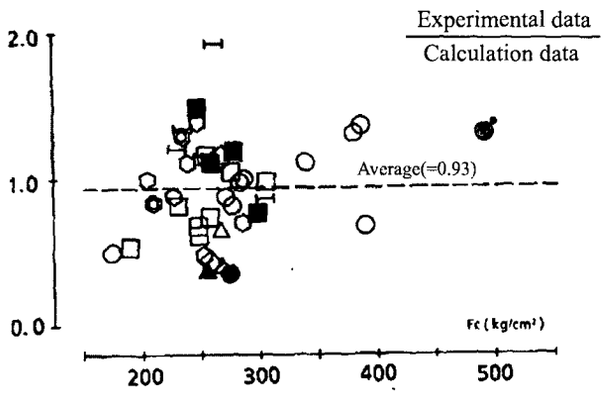

Fig.4 Comparison of initial stiffness

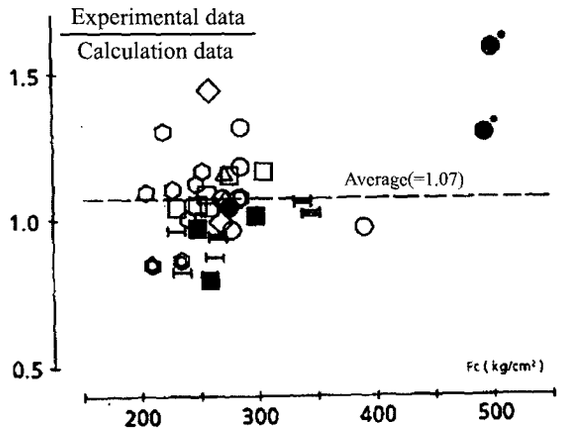

Fig.5 Comparison of second turning point M_2 (three-turning point polygonal line approximation of experimental values)

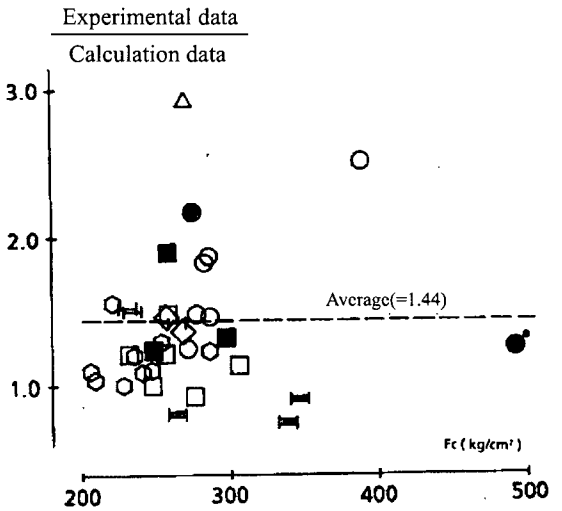

Fig.6 Comparison of second turning point R_B (three-turning point polygonal line approximation of experimental values)

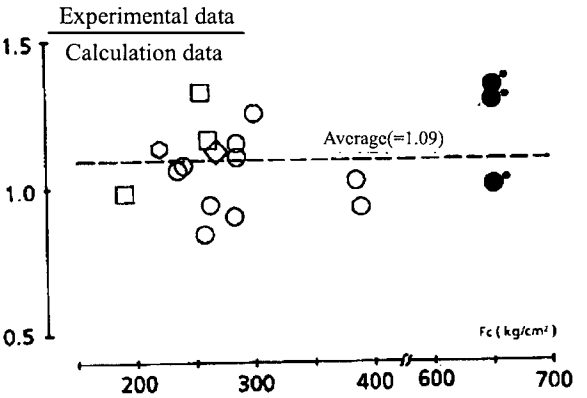

Fig.7 Comparison of ultimate bending load

2149

Evaluation Method for Restoring Force Characteristics of R/C Shear Walls of Reactor Buildings

Part 5 : Fitness Evaluation of the Computed Skeleton Curves with Experimental Data

Katsuhiko Emori[*1] (member), Hiroshi Tanaka[*2] (member)

1. Introduction

In this report, the conformity between the experimental data and the evaluation formulae for each turning point of the τ - γ and M- ϕ restoring force characteristics proposed in (Part 1) is discussed with regard to the results of a comparative investigation of the agreement with the τ - γ , M- ϕ and Q- δ skeleton curves.

2. Details of Investigation

1) τ - γ skeleton curve: Figure 1 shows an example that the experimental values obtained from a test structure compare with the calculated values.

As a method for investigating the conformance, instead of examining each turning point of the three vertices polygonal line, we compared the areas enclosed between the X axis and the actual and calculated values as shown in Fig. 2. This allowed us to comprehensively evaluate the three vertices. When the maximum deformation differs between the experimental and calculated values, they are compared based on the area up to the smaller of the two deformations. The comparison of areas was performed for experimental values in the positive force application direction. Figure 3 shows the results of comparing the areas enclosed by the skeleton curves for test structures with different cross-sectional profile. This figure shows that the curves for the experimental values enclose a larger area for box walls, I-section walls and truncated conical walls, while in cylindrical and octagonal walls the curves for the calculated values have a larger area. For the box wall with oblique force application, since there were two test

structures, it is not possible to discuss any clear trends. Overall, the ratio of the areas is close to 1, which shows that the shapes of the curves are well matched.

2) M-R_B skeleton curve: Similarly, Fig. 4 shows a comparison of the experimental and calculated values for typical test structures, and Fig. 5 shows the results of comparing the areas for each cross-sectional profile of the test structures.

Overall, the areas enclosed by the calculated values are larger, which is because compared with the skeleton curves of the calculated values, the curves of the experimental values exhibit larger deformation in the vicinity of the bending yield point.

3) Load (Q) vs. horizontal deformation (δ) skeleton curve: Similarly, Fig. 6 shows a comparison of the experimental and calculated values for typical test structures, and Fig. 7 shows the area comparison results. In the calculations, the horizontal deformation of the test structures is obtained by adding together the shear deformation obtained from the τ - γ relationship, the bending deformation obtained from the M- ϕ relationship, and the rotational deformation of the concrete footings that is considered as a special case in the scale model experiments. The area enclosed by the curves obtained by calculation is about 20% larger than the area enclosed by the experimental values, but the other shapes are matched well.

3. Summary

The skeleton curves based on the formula for the evaluation of restoring force characteristics match well to the experimental values. Although there were some test structures for which the experimental area values were smaller than the calculated values, these only accounted for a small part of the calculations area, and the actual area of the skeleton curve for experimental values (the energy absorption capacity) was sufficiently large.

*1: Kajima Corporation

*2: The Tokyo Electric Power Company

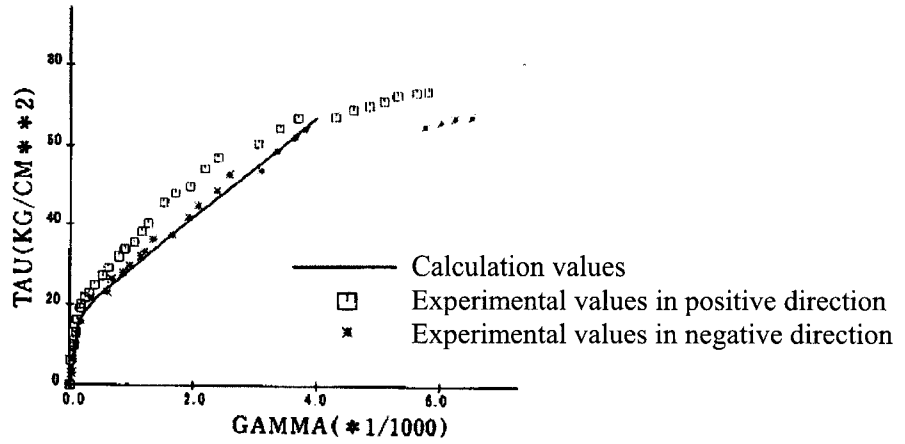

a) Cylindrical wall

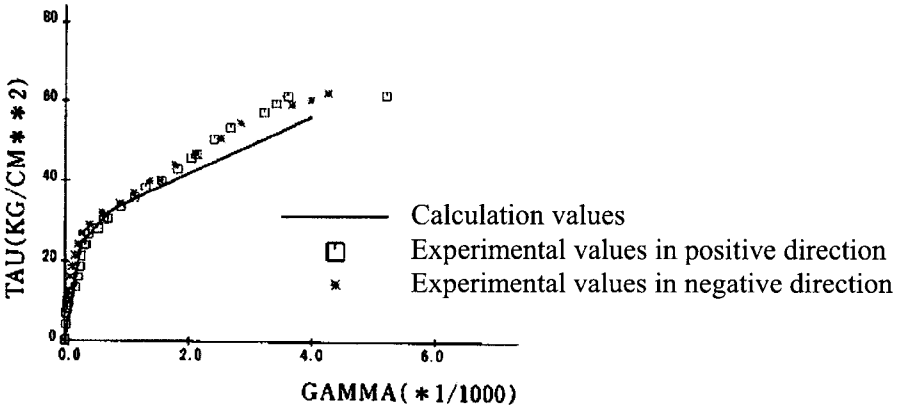

b) I-section wall

Fig.1 Example of a comparison between experimental values and calculated values of the τ-γ relationship (References 15 and 16 of Part 2)

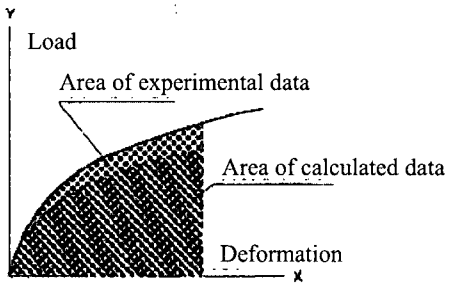

Fig.2 Comparison of areas enclosed by skeleton curves

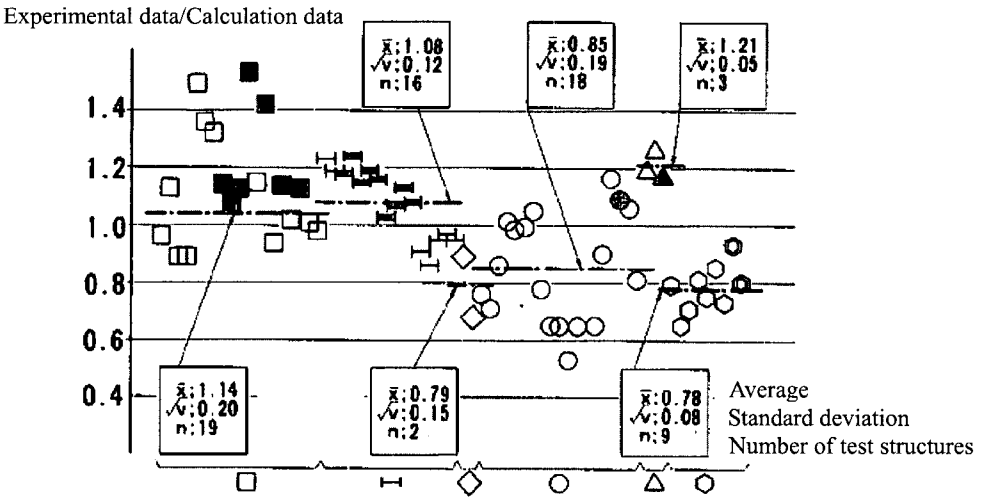

Fig.3 Comparison of areas enclosed by skeleton curves

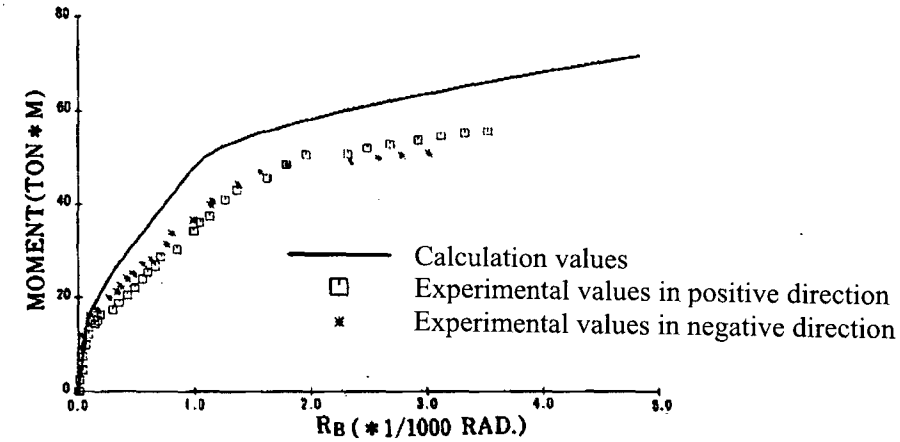

Experimental data/Calculation data

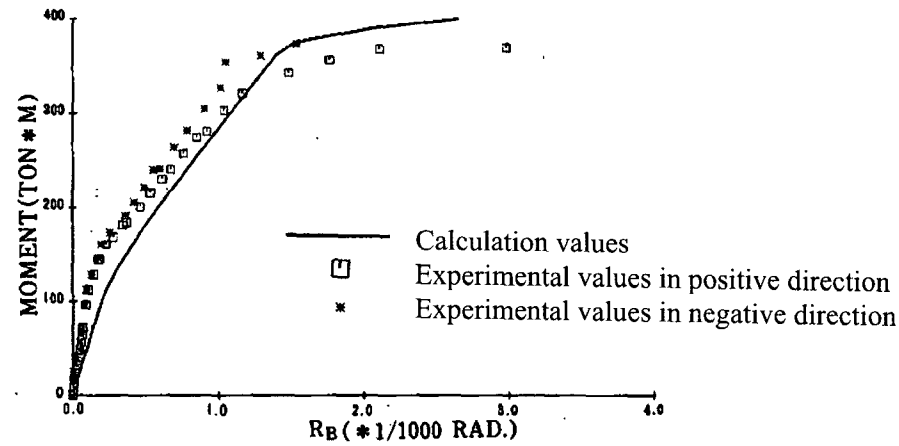

b) I-section wall

Fig.4 Example of a comparison between experimental values and calculated values of the M-R_B relationship (References 15 and 16 of Part 2)

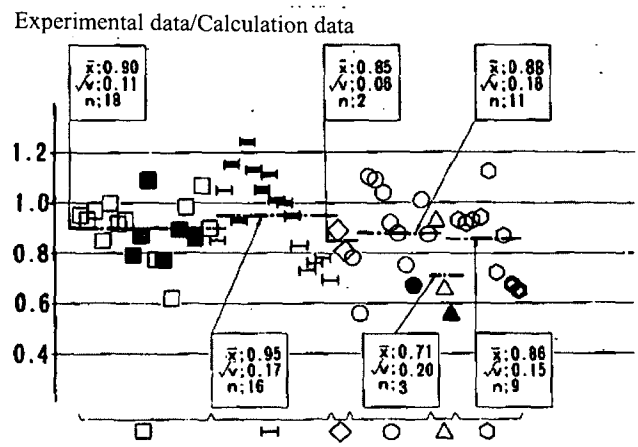

Cross-sectional figure

Fig.5 Comparison of areas enclosed by M-R_B skeleton curves

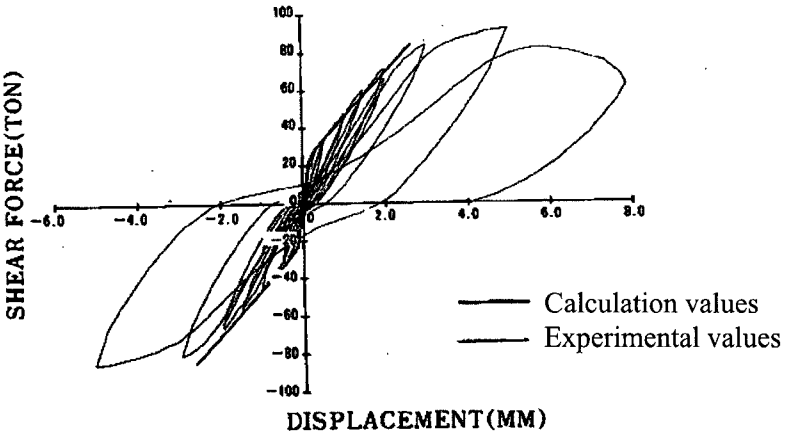

a) Cylindrical wall

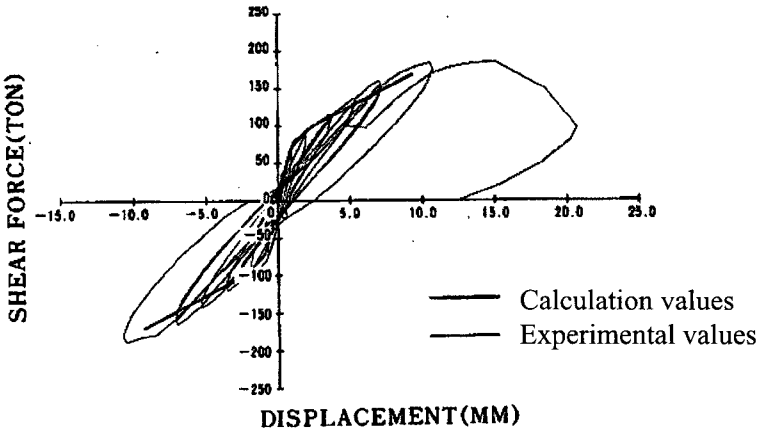

b) I-section wall

Fig.6 Example of a comparison between experimental values and calculated values of the Q- δ relationship (References 15 and 16 of Part 2)

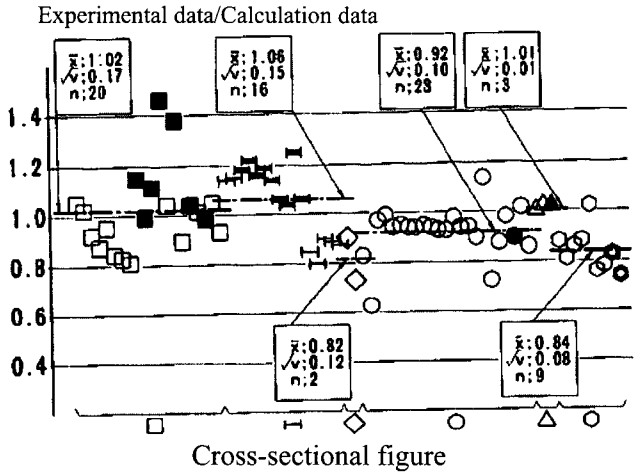

Fig.7 Comparison of areas enclosed by Q- δ skeleton curves

2150

Evaluation Method for Restoring Force Characteristics of R/C Shear Walls of Reactor Buildings

Part 6 : Hysteresis

Akira Shimizu[*1] (member), Hiroshi Tanaka[*2] (member)

1. Introduction

This report discusses restoring force evaluation methods proposed in (Part 1) that can be used for the evaluation of hysteresis characteristics.

2. Hysteresis of Shear Stress-Strain (τ - γ) Relationship

The τ - γ hysteresis were assumed to be peak-oriented, with no hysteresis damping in the stable loop. This hysteresis is determined in consideration of factors such as the range of shear strain used in the design, and the convenience of response analysis such as avoiding sudden changes associated with movements of the loop.

The loop of the τ - γ relationship is determined according to the following rules:

1) No loop is drawn in the first stiffness zone.

2) For the second and third stiffness zones, as shown in Fig. 1, the steady state moves in a straight line between the maximum and minimum values, and no loop is drawn. The first time the first turning point is exceeded, the steady state moves along the skeleton curve. At this time, the shear strain (γ) when the speed is reversed is taken to be the maximum shear strain (γ_{max}), and at the same time the shear strain at the first turning point in the negative direction ($-\gamma_1$) is taken to be the minimum shear strain (γ_{min}). Thereafter, γ_{max} and γ_{min} are sequentially updated.

3. Hysteresis of Bending Moment vs. Bend Curvature (M- ϕ) Relationship

The hysteresis characteristics of the M- ϕ relationship are assumed to be peak-oriented, with no area in the stable loop before flexural yield (in the first and second stiffness zones), and with hysteresis damping only in the third stiffness zone.

The loop of the M- ϕ relationship is determined according to the following rules.

1) No loop is drawn in the first stiffness zone.

2) In the second stiffness zone, as shown in Fig. 2, the steady state moves in a straight line between the maximum and minimum values, and no loop is drawn. The first time the first turning point is exceeded, it moves along the skeleton curve, the bend curvature (ϕ) when the speed is reversed is taken to be the maximum bend curvature (ϕ_{max}), and at the same time the first turning point bend curvature in the negative direction ($-\phi_1$) is taken to be the minimum bend curvature (ϕ_{min}). Thereafter, ϕ_{max} and ϕ_{min} are sequentially updated.

3) In the third stiffness zone, as shown in Fig. 1, the steady state describes a point-symmetrical parallelogram with its centroid at the central point of the line connecting the maximum and minimum values. As shown in Fig. 3(a), the first time the second turning point is exceeded, the steady state moves along the skeleton curve, the bend curvature (ϕ) when the speed is reversed is taken to be the maximum bend curvature (ϕ_{max}), and at the same time the second turning point bend curvature in the negative direction ($-\phi_2$) is taken to be the minimum bend curvature (ϕ_{min}). Thereafter, ϕ_{max} and ϕ_{min} are sequentially updated. The stable loop is as shown in Fig. 3(b).

The stable loop vertices and stiffness in the third stiffness zone are obtained by the following formula according to the symbols shown in Fig. 3(b), where M_1 is the bending moment at the first turning point, ϕ_{max} and ϕ_{min} are the maximum and minimum bending curvatures respectively, and M_{max} and M_{min} are the maximum and minimum bending moments respectively.

$$\phi_A = \frac{\phi_{max} \cdot M_L - \phi_L \cdot M_E + 0.5\pi \cdot \phi_L \cdot M_L \cdot he}{M_L}$$

$$M_A = M_{max} - M_E \ , \quad \phi_B = \phi_{min} + M_E / K_2$$

$$M_B = M_{min} + M_E$$

$$K_1 = \frac{M_L - M_E}{\phi_L \cdot K_2 - M_E} \cdot K_2 \ , \ K_2 = \frac{M_E}{\phi_{max} - \phi_A}$$

Here

$M_E = 2M_1$; Moment in first turning point

$\phi_L = \phi_{max} - \phi_{min}$, $M_L = M_{max} - M_{min}$

he ; Equivalent viscous damping factor

Equivalent viscous damping factor h_e is defined as Fig.4 and under formula which is function of maximum curvature as Fig.5.

$$he = 0.15 \frac{\phi_{max} - \phi_2}{\phi_3 - \phi_2}$$

Furthermore, the maximum value is defined as under formula, because the values of K_2 are never larger than first stiffness.

$$he \leqq \frac{4 (\phi_L \cdot M_1 - \phi_1 \cdot M_L)}{\pi \cdot \phi_L \cdot M_L}$$

Up to the bending yield point ($\phi \leq \phi_2$), the equivalent viscous damping factor h_e is set to zero in consideration of the situation whereby a fixed viscous damping is applied in the elastic region when performing dynamic response calculations. Of the test structures for reactor buildings, Fig. 6 shows the values of h_e and curvature ϕ for those for which it was possible to obtain a bending deformation hysteresis loop. Hardly any of these test structures were subjected to repeated loading after flexural yield, and this data can be considered to apply to the conditions before flexural yield occurs. The mean and standard deviation are 5.17% and 2.62% respectively, and the 95% confidence lower limit is 0.87%. Beyond the bending yield point ($\phi > \phi_2$), h_e is obtained with reference to experiments on an ordinary earthquake-resistant wall (Experiment 1) and column (Experiment 2) that have undergone flexural failure. In these results, h_e increases beyond flexural yield, and reaches 15–20% in the vicinity of deformation member angles of 5/1000–10/1000. According to this proposal, h_e is set so as to achieve a value of 15% at the ultimate bending to be on the safe side. With regard to the setting of the equivalent viscous damping factor, there is probably still room for further study.

Although no data is shown for the equivalent viscous damping factor of the τ - γ relationship, the setting value h_e =0 after the first turning point is determined for similar reasons to the M- ϕ relationship.

As shown in Fig. 7, repetition in the loop assumes a stiffness of K2 in a stable loop, and after a stable loop has been reached it moves along the stable loop.

4. Summary

With this evaluation method, we have obtained practical hysteresis loops that can be used for response analysis.

(References)

1. Shiga et al.: "A study of earthquake damage in reinforced concrete earthquake-resisting walls and the effects of repairs (Part 3)," AIJ Tohoku Research Proceedings, pp. 217–220, March 1983
2. Higashi et al.: "A comprehensive study on the prevention of collapse in reinforced concrete columns (Part 39)," AIJ Conference Abstracts, pp. 1421–1422, 1976

*1: Obayashi Corporation

*2: The Tokyo Electric Power Company

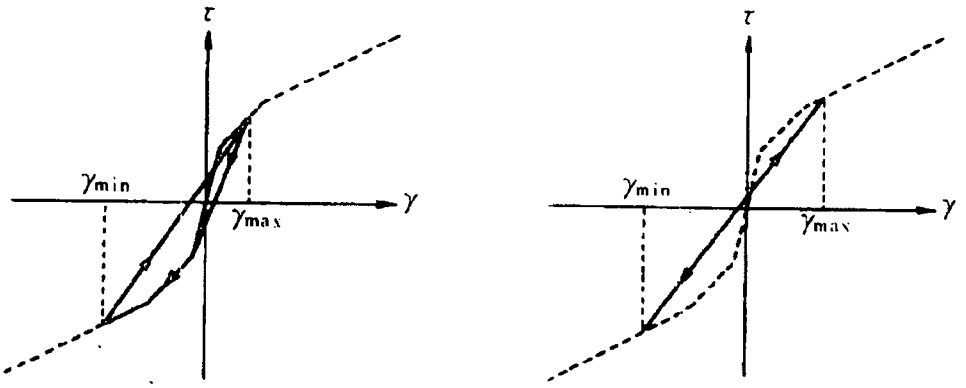

(a) Transient state (b) Steady state

Fig.1 Rules in second and third stiffness zones

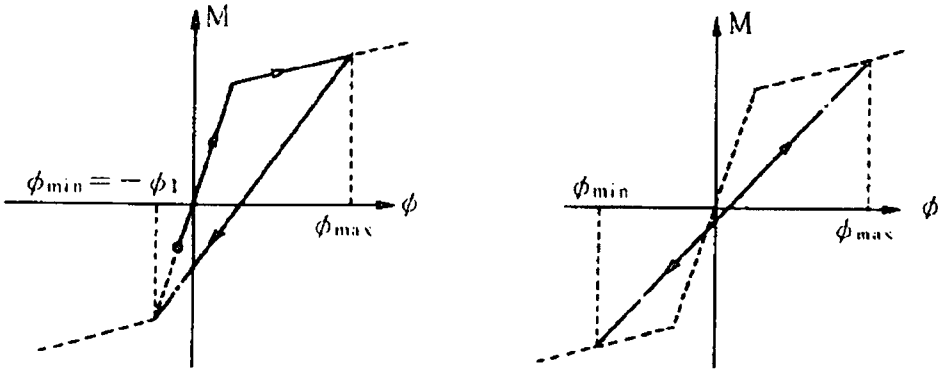

(a) When $\phi_{max} > \phi_1$ for the first time (b) Stable loop

Fig.2 Rules in second stiffness zone

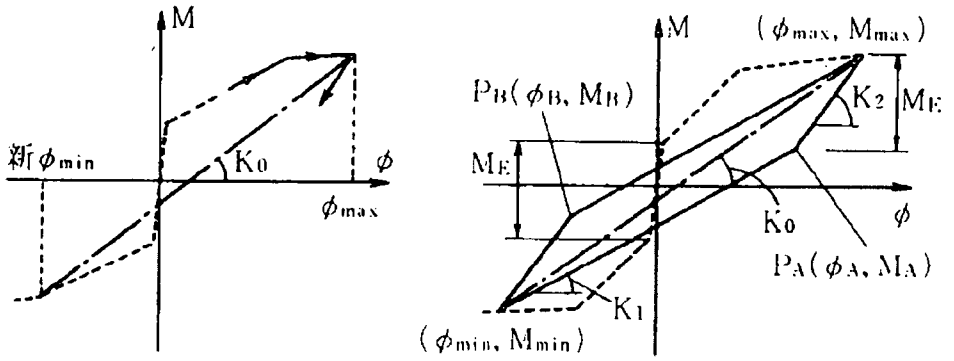

(a) When $\phi_{max} > \phi_2$ for the first time (b) Stable loop

Fig.3 Equivalent stiffness and rules in third stiffness zone

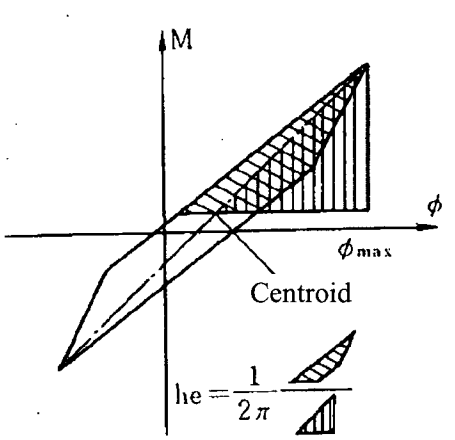

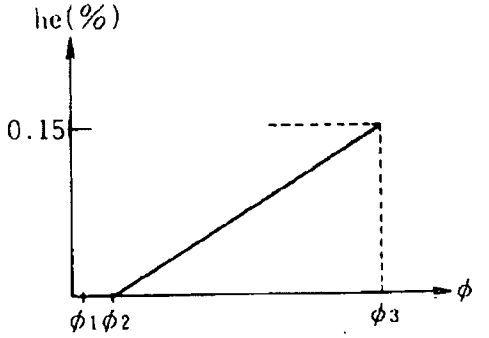

Fig.5 he- ϕ relationship in setting model

Fig.4 Definition of equivalent viscous damping factor he

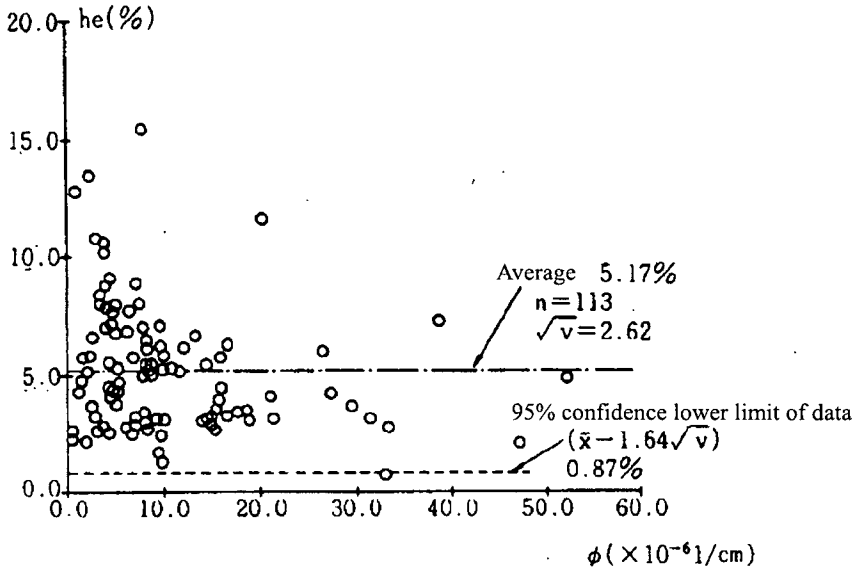

Fig. 6: Equivalent viscous damping vs. bend curvature (for ϕ max$\leq \phi_2$)

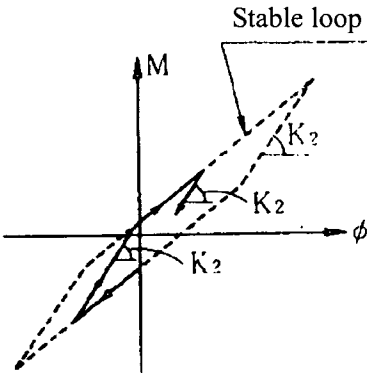

Fig.7 Cyclic in stable loop